



RESEARCH LETTER

10.1002/2016GL069323

Key Points:

- Strong semiannual variability
- Significant correlation between current and salinity
- Semiannually reversing water exchange

Supporting Information:

- Supporting Information S1

Correspondence to:

F. Wang,
fwang@qdio.ac.cn

Citation:

Wang, F., et al. (2016), Semiannually alternating exchange of intermediate waters east of the Philippines, *Geophys. Res. Lett.*, 43, 7059–7065, doi:10.1002/2016GL069323.

Received 25 APR 2016

Accepted 18 JUN 2016

Accepted article online 22 JUN 2016

Published online 2 JUL 2016

Semiannually alternating exchange of intermediate waters east of the Philippines

Fan Wang^{1,2}, Lina Song^{1,3}, Yuanlong Li^{1,4}, Chuanyu Liu^{1,2}, Jianing Wang^{1,2}, Pengfei Lin⁵, Guang Yang⁶, Jun Zhao¹, Xinyuan Diao¹, Dongxiao Zhang⁷, and Dunxin Hu^{1,2}

¹Key Laboratory of Ocean Circulation and Waves, Institute of Oceanology, Chinese Academy of Sciences, Qingdao, China, ²Function Laboratory for Ocean Dynamics and Climate, Qingdao National Laboratory for Marine Science and Technology, Qingdao, China, ³University of Chinese Academy of Sciences, Beijing, China, ⁴Department of Atmospheric and Oceanic Sciences, University of Colorado, Boulder, Colorado, USA, ⁵State Key Laboratory of Numerical Modeling for Atmospheric Sciences and Geophysical Fluid Dynamics, Institute of Atmospheric Physics, Chinese Academy of Sciences, Beijing, China, ⁶Center for Ocean and Climate Research, First Institute of Oceanography, State Oceanic Administration, Qingdao, China, ⁷Joint Institute for the study of the Atmosphere and Ocean, University of Washington and NOAA/Pacific Marine Environmental Laboratory, Seattle, Washington, USA

Abstract Intermediate water exchange in the northwest tropical Pacific is explored with the temperature, salinity, and current measurements of a mooring system deployed at 8°N, 127.05°E during 2010–2014. For the first time, prominent semiannual variability (SAV; with the maximum power at ~ 187 days) of subthermocline meridional flow along the Mindanao coast is revealed. A significant correlation between meridional flow and salinity is found at intermediate depths. This provides direct evidence for the alternating transports of South Pacific and North Pacific Intermediate Waters by northward and southward undercurrents, respectively. Further analysis with an eddy-resolving ocean general circulation model demonstrates that the SAV is generated locally near the western boundary, manifesting as large-scale subthermocline recirculation and leading to alternating northward and southward flows near the Mindanao coast, which plays an efficient role in the intermediate water exchange of the northwest tropical Pacific. Mechanisms underlying the observed SAV are discussed.

1. Introduction

The northwest tropical Pacific Ocean is a key region for intergyre, interhemisphere, and interbasin exchanges of mass, heat, and freshwater [Fine et al., 1994; Talley, 2013]. In the intermediate layer of the Pacific, both the North Pacific Intermediate Water (NPIW) and the Antarctic Intermediate Water (AAIW) form in the midlatitudes and high latitudes of the Northern and Southern Hemispheres, respectively, and spread equatorward [Reid, 1965; Talley, 1993]. As vertical salinity minima [Reid, 1965; Talley, 1993], the NPIW (salinity ~ 34.28 psu (practical salinity units)) is identified at ~26.7–26.8 kg m⁻³ potential density surface (σ_θ) and the AAIW (salinity ~ 34.53 psu) at ~27.2 σ_θ (Figure 1). The NPIW can reach as far south as 8°N along the western boundary of the Pacific basin [Bingham and Lukas, 1994; Fine et al., 1994], while the AAIW intrudes farther north across the equator [Reid, 1997; Talley, 1993, 1999] and can be traced by its characteristic properties to approximately 15°N [Qu and Lindstrom, 2004; Reid, 1965]. The two water masses meet in the northwest tropical Pacific, where they spread to the central and eastern Pacific via equatorial currents and the Indian Ocean via the Indonesian throughflow [Bingham and Lukas, 1994, 1995; Fine et al., 1994; Tsuchiya, 1991]. However, the specific exchange processes between the two waters remain unclear.

Previous studies hypothesized that equatorward movements of the intermediate waters are linked to low-latitude western boundary currents in the convergence region [Bingham and Lukas, 1994; Fine et al., 1994; Kashino et al., 1996; Lindstrom et al., 1987; Qu and Lindstrom, 2004; Schönau et al., 2015; Wang and Hu, 1998; Zenk et al., 2005]. The southward Mindanao Current (MC) transports the NPIW southward between 26.0 and 27.0 σ_θ [Bingham and Lukas, 1994; Fine et al., 1994], while the AAIW is carried to the western Pacific by the northwestward and transequatorial New Guinea Coastal Undercurrent (NGCUC) [Kashino et al., 1996; Lindstrom et al., 1987; Qu and Lindstrom, 2004; Zenk et al., 2005]. Along the western boundary, the Mindanao Undercurrent (MUC) transports South Pacific water farther north [Qu and Lindstrom, 2004; Schönau et al., 2015; Wang and Hu, 1998; Wang et al., 2015] than in the interior Pacific Ocean. However, these hypothesized relationships between currents and water masses in the intermediate layer are primarily

©2016. The Authors.

This is an open access article under the terms of the Creative Commons Attribution-NonCommercial-NoDerivs License, which permits use and distribution in any medium, provided the original work is properly cited, the use is non-commercial and no modifications or adaptations are made.

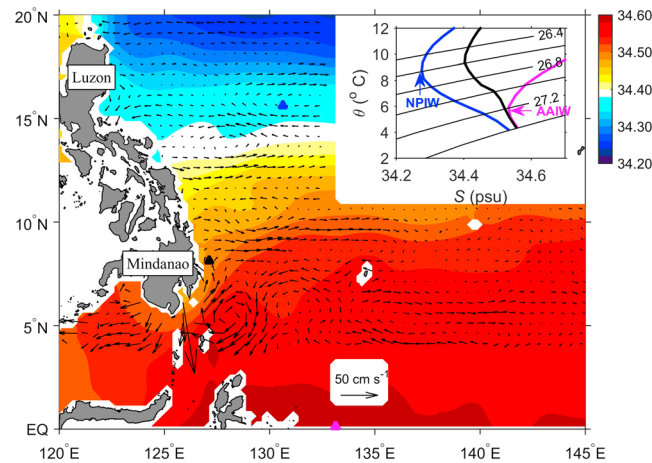


Figure 1. Annual mean climatological salinity (color shading; in psu) and geostrophic velocity (arrows; in cm s^{-1}) at $27.0\sigma_\theta$. θ - S diagrams from WOA13 annual climatology of three representative locations are inserted. The blue curve is for 15.5°N , 130.5°E (blue triangle), representing the profile of NPIW; the magenta curve is for 0°N , 133°E (magenta triangle), representing the AAIW profile; and the black curve is for 8°N , 127°E , near the mooring site (black triangle; 8°N , 127.05°E).

800 m, from 1 December 2010 to 27 August 2014. Details of this subsurface mooring system (Figure S1) are provided in the supporting information.

2. Observed Variability of the Undercurrent

Our analysis reveals both expected and unexpected variations in current and water properties that deviate dramatically from the known climatologic structure (Figures 2a and 2b). Underneath the stable southward flowing MC (which is confined to the upper 300 m throughout the observation period), the measured undercurrent alternates northward (red color) and southward (blue color) between 400 and 800 m (Figure 2a). With pronounced variations and frequent reversals, the meridional current reaches as large as $40\text{--}50 \text{ cm s}^{-1}$ during the northward periods and peaks at $20\text{--}30 \text{ cm s}^{-1}$ during the southward periods. The mean undercurrent velocity of $< 10 \text{ cm s}^{-1}$ is likely the long-term remnant of north and south reversals that are asymmetric in intensity. The pronounced undercurrent variability and its role in intermediate water mass exchange is the focus of the present study.

Figures 2c and 2d show the wavelet analysis for the meridional current averaged over $26.8\text{--}27.2\sigma_\theta$, capturing the characteristics of the intermediate current variability. The variability power generally increases with period, showing two significant power peaks. One falls between 140 and 240 day periods, representing the semi-annual variability (SAV), with the power maximum at ~ 187 days. The other denotes intraseasonal variability (ISV), with a power maximum at ~ 66 days. The striking SAV of the intermediate flow in this region is reported for the first time. The SAV was particularly strong since July 2012 (Figure 2c), while before that date, it failed to pass the 95% significant level but still had larger power than ISV. It should be noted that in spite of the power maximum at 187 days, the power is prevalently large between 140 and 240 days, and the error bar is rather large. In fact, the “SAV” addressed here refers broadly to the large variability with periods evidently longer than ISV (e.g., > 120 days) and shorter than annual variation (e.g., < 260 days). In the following, we will show that the SAV plays an active role in the meridional exchange of intermediate waters. The ISV is significant during September 2011 to April 2012 and October 2012 to June 2013. This further confirms the earlier findings of Zhang *et al.* [2014] that during December 2010 to December 2012 the ISV shows a typical period of 60–80 days. Previous studies argued that the pronounced ISV was mainly caused by subthermocline mesoscale eddies [Chiang and Qu, 2013; Qu *et al.*, 2012; Wang *et al.*, 2014] and seemed to be a common feature of the western boundary undercurrents in the tropical and subtropical oceans [e.g., Beal and Bryden, 1997; Lindstrom *et al.*, 1987; Stramma *et al.*, 1995]. Besides eddies, tides may also affect current variability. We then recompute the spectral power with hourly acoustic Doppler current profiler (ADCP) records and find

based on synoptic observations, including conductivity-temperature-depth data (CTD), expendable bathythermograph measurements (XBT), and glider data [Bingham and Lukas, 1995; Kashino *et al.*, 1996; Schönau *et al.*, 2015]. Few attempts have been made to confirm this hypothesis through measurements, combining either water properties and velocities, or long-term continuous observational time series to determine any temporal variability.

For the first time, we have been able to obtain insights into the variability and detailed exchange processes between intermediate waters with nearly 4 years of continuous measurements. A subsurface mooring was deployed at 8°N , 127.05°E (within the convergence region, Figure 1) to monitor temperature, salinity, and current of the upper

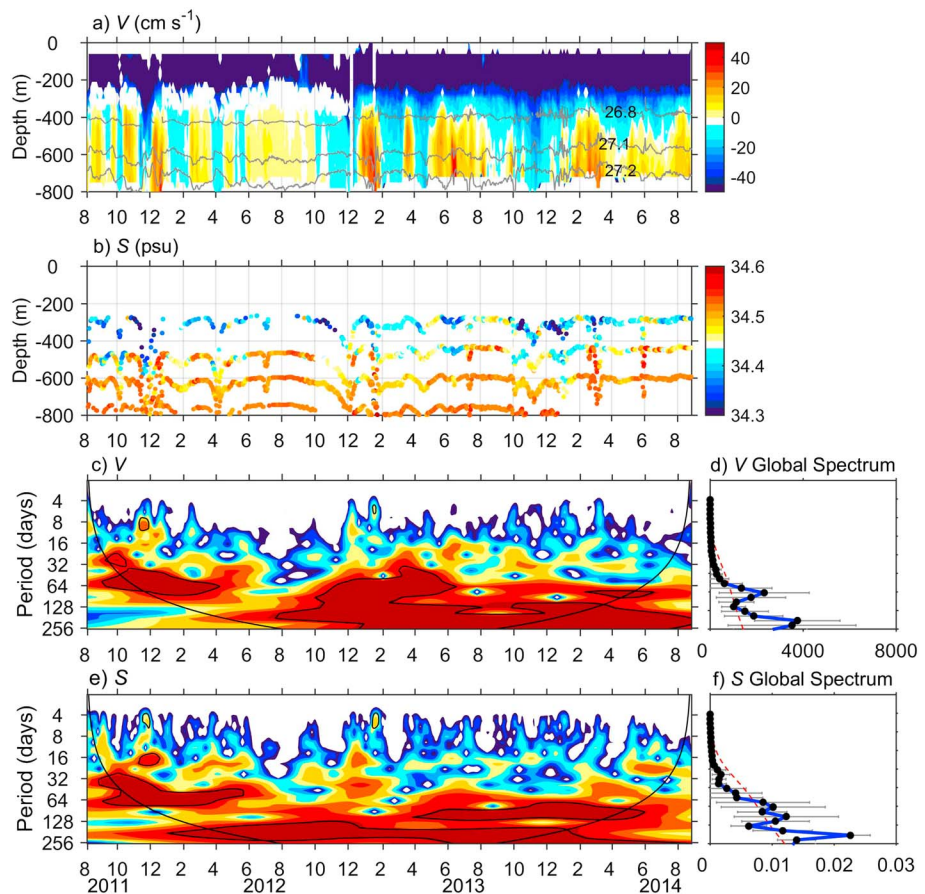


Figure 2. (a) ADCP-measured meridional velocity V (cm s^{-1}) during August 2011 to August 2014 from the mooring at 8°N , 127.05°E . Grey curves denote the isopycnals of 26.8 , 27.1 , and $27.2\sigma_{\theta}$. (b) Salinity S records (psu) measured by the CTs and CTDs (designed at 400 , 550 , 700 , and 850 m) from the mooring. (c) Wavelet power spectrum for V averaged between 26.8 and $27.2\sigma_{\theta}$. The thick black contours represent 95% significance level. (d) The corresponding global power spectrum of Figure 2c, where the red dashed line denotes the 95% significance level, and the grey bars indicate 1 standard deviation range. (e and f) The same as Figures 2c and 2d but for S averaged between 26.8 and $27.2\sigma_{\theta}$.

that V variance at major tide frequencies (semidiurnal, diurnal, and fortnight) is at least 1 order weaker than SAV and ISV. Therefore, tidal rectification is not likely to have a large impact on the observed SAV and ISV.

Salinity records from four conductivity sensors of the mooring also show prominent SAV with a peak at ~ 187 days and ISV between 66 and 94 days (Figures 2e and 2f). The power difference between SAV and ISV is even larger in S . Interestingly, there is a discernible correspondence between S and V variations in Figures 2a and 2b. That is, northward currents tend to carry saltier water, while the southward currents tend to carry fresher water. For instance, the northward currents during June–October 2012, May–August 2013, and February–August 2014 all correspond to higher salinity ($S > 34.50$ psu) between 500 and 800 m. Similarly, southward flows during October–December 2012, February–May 2013, and October 2013 to February 2014 correspond approximately to lower salinity packages ($S < 34.50$ psu). Meridional current and salinity show positive correlations between 350 and 750 m, with the maximum coefficient of 0.32 at 570 m, which exceeds 95% confidence level, assuming that effective degrees of freedom is 46 .

3. Exchange of the Intermediate Waters

As the primary tracer of intermediate waters, salinity is an indicator for intermediate water exchange process. In order to identify the relationship between salinity variations and current reversals, we plot potential temperature-salinity (θ - S) scatter in Figure 3a. In addition, typical θ - S diagrams for the NPIW (at 15.5°N , 130.5°E) and AAIW (at 0°N , 133°E) taken from the World Ocean Atlas 2013 (WOA13) annual climatology

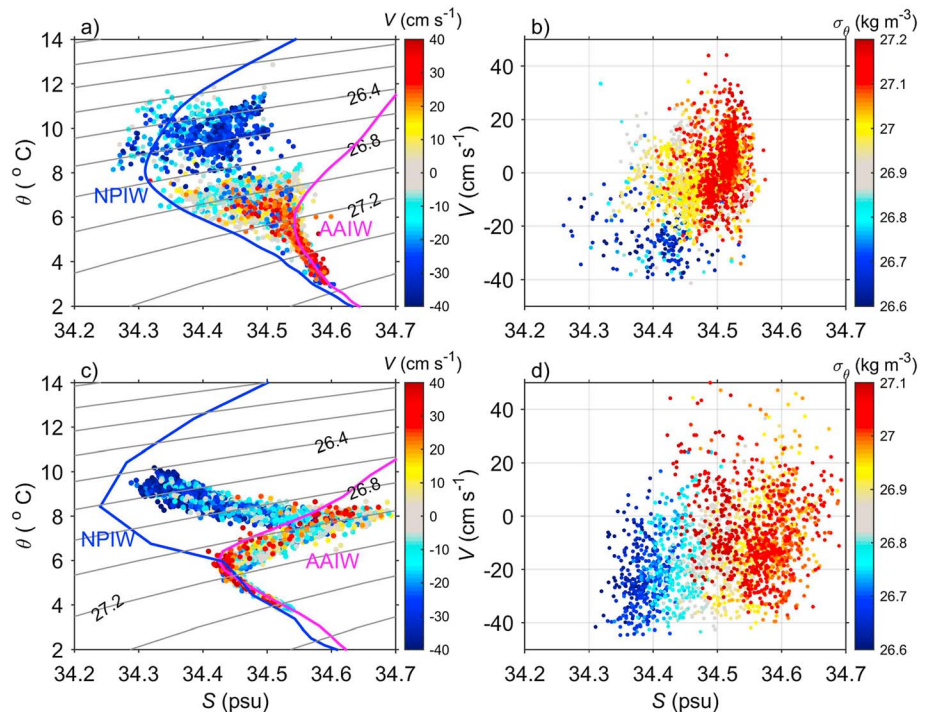


Figure 3. The relationship between the undercurrent and water mass property in the intermediate layer. (a) Scatterplot of measured potential temperature (θ) against salinity (S). The color denotes ADCP-measured V (in cm s^{-1}). The blue and magenta curves show representative θ - S diagrams for the NPIW and AAIW, respectively (as in Figure 1). (b) Scatterplot of the measured V - S at 26.6 – $27.2\sigma_\theta$, between the vertical minima of NPIW and AAIW. The color denotes potential density (σ_θ ; in kg m^{-3}), derived from CT/CTDs. (c and d) The same as Figures 3a and 3b but from OFES results.

[Locarnini *et al.*, 2013; Zweng *et al.*, 2013] are also shown for reference. The NPIW features salinity < 34.45 psu between 26.4 and $27.0\sigma_\theta$, while the AAIW is characterized by $S > 34.5$ psu between 26.9 and $27.3\sigma_\theta$. Figure 3a also demonstrates that most of the southward currents (blue dots) carry waters with evident NPIW signatures, while the waters carried by strong northward currents (red dots) conform to the typical AAIW diagram. The salinity of the NPIW observed here is consistent with the WOA13 diagram near the mooring site (black curve in Figure 1) and saltier than the typical NPIW diagram at 15.5°N , 130.5°E by 0.05 – 0.10 psu, reflecting the strong mixing along the Philippine coast [e.g., Bingham and Lukas, 1994; Li and Wang, 2012]. Weak currents (grey dots) carry waters with mixed NPIW and AAIW properties (34.4 – 34.5 psu and 26.8 – $27.2\sigma_\theta$). Redrawing the data points in V - S space (Figure 3b) further confirms the above relationship. These results suggest that the fresher water NPIW is carried by the southward current and the saltier AAIW is transported by the northward flowing current. It is worth mentioning that waters with AAIW characteristics are occasionally carried by southward currents (blue dots follow AAIW curve above $27.2\sigma_\theta$ in Figure 3a; red dots with negative velocities in Figure 3b), implying that some of the AAIW is not sufficiently mixed with local water before being taken back to the south by the recirculation and the southward flowing flank of eddies [Firing *et al.*, 2005; Qu *et al.*, 2012; Wang *et al.*, 2014].

Next we examine, between the ISV and SAV, on which timescale intermediate waters are more efficiently exchanged. Low-pass and high-pass filters with a cutoff period of 100 days were applied to vertical-averaged meridional velocity and salinity, to distinguish the SAV and ISV, respectively (Figure S2). It is found that the correlation between meridional velocity and salinity is higher for the SAV ($r=0.36$) than for ISV ($r=0.25$) or the unfiltered data ($r=0.28$). Furthermore, the correlation coefficient for SAV is largest ($r=0.49$) when salinity lags current by 34 days (Figure S3). This 34 day lag reflects the response time of local salinity to the forcing of anomalous current advection at semiannual timescale. These results suggest that the intermediate water exchange by current reversals is particularly efficient on semiannual timescale.

Mooring measurements at a single point are far from sufficient for fully understanding the current-water mass relationship. Therefore, we further employ the output of the $0.1^\circ \times 0.1^\circ$ ocean general circulation model

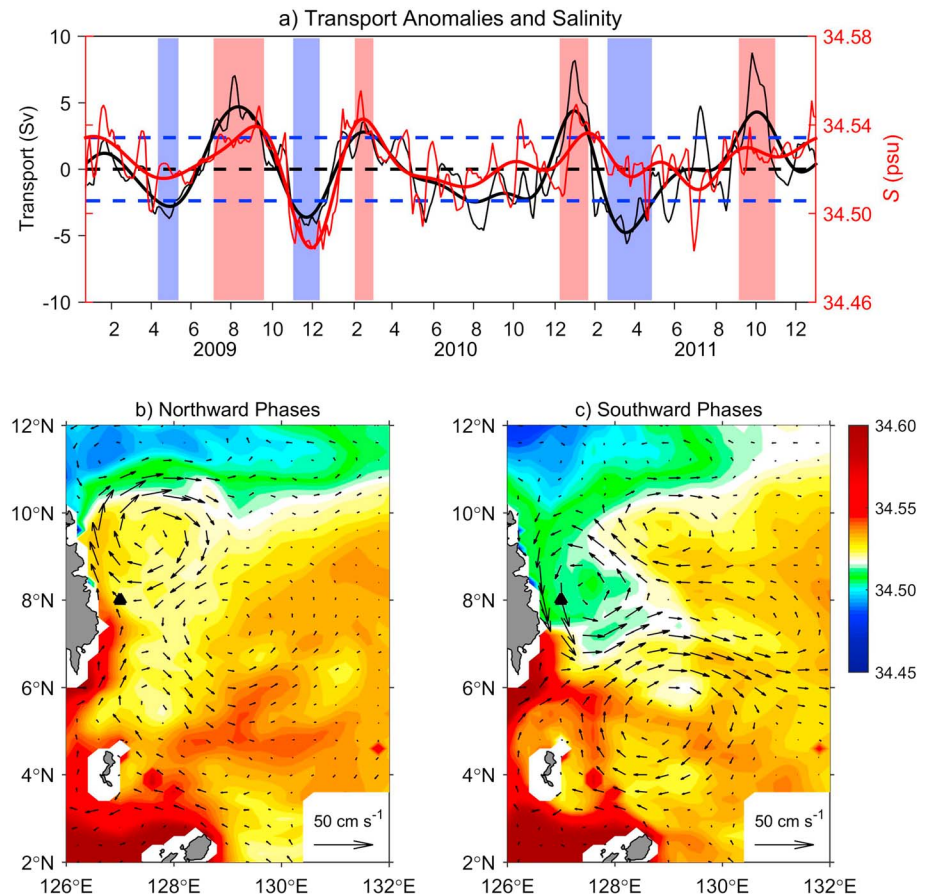


Figure 4. Water mass exchange and its relationship to circulation off the Mindanao coast. (a) Meridional transport anomalies (black lines; 1 Sv (sverdrup) = $10^6 \text{ m}^3/\text{s}$) and salinity (red lines) between 126.6 and 127.2°E , 26.8 – $27.1\sigma_\theta$ at 8°N in 2009–2011 from OFES outputs. The thin lines are original daily data, while the thick lines are 100 day low-pass filtered data. Red and blue phases are defined as periods with the transport anomaly larger than 1 (northward) and smaller than -1 (southward) standard deviation, respectively. (b) Composite map of salinity (color shading) and current (black arrows) for the northward phase. (c) The same as Figure 4b but is the composite map for the southward phase.

for the Earth Simulator (OFES) [Masumoto *et al.*, 2004; Sasaki *et al.*, 2004]. The consistency between model and mooring results is first examined. The θ - S relations of the NPIW/AAIW (Figures 3c and 3d) and the southward/northward undercurrents (Figure 4a) are faithfully captured by the model. In particular, the simulated salinity and undercurrents also show weak ISV with periods of 60–90 days and energetic SAV with a period of 198–236 days (Figure S4), in accordance with measured data. These results demonstrate that the model is able to reasonably represent the processes associated with the SAV in the intermediate layer. Using the OFES results, we can construct composite patterns at different SAV phases. Figures 4b and 4c show the composite circulation and salinity for the northward and southward phases at 26.8 – $27.1\sigma_\theta$, averaged over periods when the 100 day low-pass filtered transport anomalies are positive and negative, respectively, and the absolute value of the transport anomaly is larger than 1 standard deviation. Northward and southward phases are denoted as red and blue shadings in Figure 4a.

During the northward phases, a continuous northward flowing undercurrent emerges between 3° and 11°N (Figure 4b). The undercurrent is strengthened to the north by an anticyclonic recirculation northeast of Mindanao. Due to advection, the relatively saltier AAIW can intrude farther north along the western boundary and then turn east at 11°N . Meanwhile, the NPIW is confined north of 11°N . Consequently, the mooring area is dominated by the northward undercurrent and the AAIW. In contrast, during the southward phases, the Mindanao coastal area is dominated by a cyclonic recirculation pattern and the northward flowing undercurrent is confined south of 7°N (Figure 4c). The cyclonic recirculation blocks the northward intrusion of the AAIW and induces eastward flow, part of which turns northward and then proceeds to 10°N in a circuitous

route. As a result, the mooring area is dominated by a southward current and NPIW properties. We also checked the circulation and salinity patterns of individual events (Figure S5), which are roughly consistent with the composite ones described here, albeit with some detailed discrepancies in intensity and structure. This means that the semiannually reversing current northeast of the Mindanao coast plays as a robust bidirectional conveyor for the undercurrent-dependent meridional water exchange. The conveyor associated with circulations affects the AAIW and NPIW intrusions in different ways: the AAIW can eventually reach 10°–11°N during both phases, carried by either straight or circuitous undercurrent routes, while the NPIW only enters the equatorial ocean semiannually during phases when cyclonic recirculation is located to the northwest.

4. Remarks and Discussion

This study utilizes long-term, continuous, and synchronous measurements of temperature, salinity, and current along the western boundary of the northwest tropical Pacific. We reveal pronounced variations of subthermocline meridional flow along the Mindanao coast at semiannual and intraseasonal timescales. A significant correlation is found between the meridional flow and salinity, and a bidirectional conveyor mechanism for efficient interhemisphere intermediate water exchange is put forward. In our mooring observation, surface-layer meridional current between 50 and 300 m also has strong SAV with a period of 187 days (Figure S6), but the correlation between surface current and intermediate current is insignificant. The OFES allows for an investigation with a longer time series. Over 2001–2011, the correlation between MC and undercurrent is $r = 0.36$ for the SAV. These results suggest that a large portion of the undercurrent variability is not consistent with the surface current. Checking the time-longitude plots of the SAV anomalies (Figures S7a and S7b) suggests that the SAV is not originated from the ocean interior but mostly generated locally along the western boundary. In addition, an inspection over the time-latitude plots (Figures S7c and S7d) indicates that the SAV anomalies show evident northward propagation tendency along the western boundary, and some of the SAV is generated to the south and get enhanced near Mindanao. This feature is similar to the case of ISV, which are in form of subthermocline eddies originating from the south [Chiang and Qu, 2013; Qu *et al.*, 2012; Wang *et al.*, 2014]. The flow patterns in Figures 4 and S5 also indicate that the SAV primarily manifests as large-scale eddies (recirculation) east of Mindanao. The generation mechanism for the subthermocline eddies are, however, difficult to clarify. They can arise from the internal instabilities of the western boundary currents, particularly the baroclinic and barotropic instabilities associated with the strong current shears [Chiang and Qu, 2013], or are partly induced by local wind forcing of the monsoon [Qu *et al.*, 2008; Zhao *et al.*, 2012]. To clarify the underlying mechanism, a solid investigation with numerical model experiments isolating effects of different candidates is demanded, which is the theme of our ongoing research.

In this study a large impact of SAV on intermediate water mass exchange is seen. In contrast, the impact of ISV on water mass exchange is much less significant. The correlation between V and S at intraseasonal timescale is not significant. A composite analysis similar to Figure 4 is conducted for ISV, and the salinity distribution shows little difference for northward and southward phases (figure not shown). Compared with SAV, the amplitude of ISV is weaker (Figure 2), and the forcing period of intraseasonal advection anomaly is too short for sufficient exchange between the AAIW and NPIW.

Our results may be indicative of a common mechanism for the interhemisphere intermediate water mass exchange around the world ocean [Talley, 2013]. Nevertheless, measurements from a single mooring are not sufficient to resolve spatial patterns in circulation or water mass properties nor their variability on different timescales. For an in-depth understanding of intermediate water mass exchange, particularly its relationship with basin-scale and global-scale climate changes, such as El Niño–Southern Oscillation, thermohaline circulation, and global water cycle, observations of longer duration and better spatial coverage are required for future research.

References

- Beal, L. M., and H. L. Bryden (1997), Observations of an Agulhas Undercurrent, *Deep Sea Res., Part I*, 44(9), 1715–1724.
- Bingham, F. M., and R. Lukas (1994), The southward intrusion of North Pacific Intermediate Water along the Mindanao coast, *J. Phys. Oceanogr.*, 24(1), 141–154.
- Bingham, F. M., and R. Lukas (1995), The distribution of intermediate water in the western equatorial Pacific during January–February 1986, *Deep Sea Res., Part I*, 42(9), 1545–1573.
- Chiang, T.-L., and T. Qu (2013), Subthermocline eddies in the western equatorial Pacific as shown by an eddy-resolving OGCM, *J. Phys. Oceanogr.*, 43, 1241–1253.

Acknowledgments

This research is supported by the National Basic Research Program of China (2012CB417401 and 2013CB956204), the Strategic Priority Research Program of the Chinese Academy of Sciences (XDA11010204), the Knowledge Innovation Program of the Chinese Academy of Sciences (Y62114101Q), the National Natural Science Foundation of China (NSFC; 40890152 and 41330963), the NSFC-Shandong Joint Fund for Marine Science Research Centers (U1406401), the Global Change and Air-Sea Interaction (GASI-03-01-01-05), and the NSFC Innovative Group grant (41421005). Comments from two anonymous reviewers are helpful for improving our manuscript. Temperature and salinity climatology of WOA13 is obtained from the NOAA National Centers for Environmental Information (NCEI) through <https://www.nodc.noaa.gov/>. The OFES simulations were conducted on the Earth Simulator and available from <http://apdrc.soest.hawaii.edu/datadoc/ofes/ofes.php>. The mooring data used in this study are available for research purpose upon request to Dr. Fan Wang (fwang@qdio.ac.cn).

- Fine, R. A., R. Lukas, F. M. Bingham, M. J. Warner, and R. H. Gammon (1994), The western equatorial Pacific: A water mass crossroads, *J. Geophys. Res.*, *99*(C12), 25,063–25,080, doi:10.1029/94JC02277.
- Firing, E., Y. Kashino, and P. Hacker (2005), Energetic subthermocline currents observed east of Mindanao, *Deep Sea Res., Part II*, *52*(3), 605–613.
- Kashino, Y., M. Aoyama, T. Kawano, N. Hendiarti, Y. Anantasena, K. Muneyama, and H. Watanabe (1996), The water masses between Mindanao and New Guinea, *J. Geophys. Res.*, *101*(C5), 12,391–12,400, doi:10.1029/95JC03797.
- Li, Y., and F. Wang (2012), Spreading and salinity change of North Pacific tropical water in the Philippine Sea, *J. Oceanogr.*, *68*, 439–452.
- Lindstrom, E., R. Lukas, R. Fine, E. Firing, S. Godfrey, G. Meyers, and M. Tsuchiya (1987), The western equatorial Pacific Ocean circulation study, *Nature*, *330*(10), 533–537.
- Locarnini, R. A., et al. (2013), World Ocean Atlas 2013, Volume 1: Temperature S. Levitus, Ed., A. Mishonov Technical Ed., NOAA Atlas NESDIS, 73, 40.
- Masumoto, Y., H. Sasaki, T. Kagimoto, N. Komori, A. Ishida, Y. Sasai, T. Miyama, T. Motoi, H. Mitsudera, and K. Takahashi (2004), A fifty-year eddy-resolving simulation of the world ocean: Preliminary outcomes of OFES (OGCM for the Earth Simulator), *J. Earth Simul.*, *1*, 35–56.
- Qu, T., and E. J. Lindstrom (2004), Northward intrusion of Antarctic Intermediate Water in the western Pacific*, *J. Phys. Oceanogr.*, *34*(9), 2104–2118.
- Qu, T., J. Gan, A. Ishida, Y. Kashino, and T. Tozuka (2008), Semiannual variation in the western tropical Pacific Ocean, *Geophys. Res. Lett.*, *35*, L16602, doi:10.1029/2008GL035058.
- Qu, T., T. L. Chiang, C. R. Wu, P. Dutrieux, and D. Hu (2012), Mindanao Current/Undercurrent in an eddy-resolving GCM, *J. Geophys. Res.*, *117*, C06026, doi:10.1029/2011JC007838.
- Reid, J. L. (1965), Intermediate waters of the Pacific Ocean, *Johns Hopkins Oceanogr. Stud.*, *2*, 1–85.
- Reid, J. L. (1997), On the total geostrophic circulation of the Pacific Ocean: Flow patterns, tracers, and transports, *Prog. Oceanogr.*, *39*(4), 263–352.
- Sasaki, H., Y. Sasai, S. Kawahara, M. Furuichi, F. Araki, A. Ishida, Y. Yamanaka, Y. Masumoto, and H. Sakuma (2004), A series of eddy-resolving ocean simulations in the world ocean-OFES (OGCM for the Earth Simulator) project paper presented at OCEANS'04. MTS/IEEE TECHNO-OCEAN'04, IEEE.
- Schönauf, M. C., D. L. Rudnick, I. Cerovecki, G. Gopalakrishnan, B. D. Cornuelle, J. L. McClean, and B. Qiu (2015), The Mindanao Current: Mean structure and connectivity, *Oceanography*, *28*(4), 34–45.
- Stramma, L., J. Fischer, and J. Reppin (1995), The north Brazil Undercurrent, *Deep Sea Res., Part I*, *42*(5), 773–795.
- Talley, L. D. (1993), Distribution and formation of North Pacific Intermediate Water, *J. Phys. Oceanogr.*, *23*(3), 517–537.
- Talley, L. D. (1999), Some aspects of ocean heat transport by the shallow, intermediate and deep overturning circulations, in *Mechanisms of Global Climate Change at Millennial Time Scales*, *Geophys. Monogr. Ser.*, vol. 112, edited by P. U. Clark, R. S. Webb, and L. D. Keigwin, pp. 1–22, AGU, Washington, D. C.
- Talley, L. D. (2013), Closure of the global overturning circulation through the Indian, Pacific, and Southern Oceans: Schematics and transports, *Oceanography*, *26*, 80–97.
- Tsuchiya, M. (1991), Flow path of the Antarctic Intermediate Water in the western equatorial South Pacific Ocean, *Deep Sea Res., Part A*, *38*, S273–S279.
- Wang, F., and D. Hu (1998), Dynamic and thermohaline properties of the Mindanao Undercurrent, part II: Thermohaline structure, *Chin. J. Oceanol. Limnol.*, *16*(3), 206–213.
- Wang, F., N. Zang, Y. Li, and D. Hu (2015), On the subsurface countercurrents in the Philippine Sea, *J. Geophys. Res. Oceans*, *120*, 131–144, doi:10.1002/2013JC009690.
- Wang, Q., F. Zhai, F. Wang, and D. Hu (2014), Intraseasonal variability of the subthermocline current east of Mindanao, *J. Geophys. Res. Oceans*, *119*, 8552–8566, doi:10.1002/2014JC010343.
- Zenk, W., G. Siedler, A. Ishida, J. Holfort, Y. Kashino, Y. Kuroda, T. Miyama, and T. J. Müller (2005), Pathways and variability of the Antarctic Intermediate Water in the western equatorial Pacific Ocean, *Prog. Oceanogr.*, *67*(1), 245–281.
- Zhang, L., D. Hu, S. Hu, F. Wang, F. Wang, and D. Yuan (2014), Mindanao Current/Undercurrent measured by a subsurface mooring, *J. Geophys. Res. Oceans*, *119*, 3617–3628, doi:10.1002/2013JC009693.
- Zhao, J., Y. Li, F. Wang, F. Zhai, and X. Yu (2012), Spatial-temporal patterns and driving mechanisms of semiannual variations in the Philippine Sea, *Deep Sea Res., Part I*, *68*, 105–115.
- Zweng, M., J. Reagan, J. Antonov, R. Locarnini, A. Mishonov, T. Boyer, H. Garcia, O. Baranova, D. Johnson, and D. Seidov (2013), World Ocean Atlas 2013. Vol. 2: Salinity S. Levitus, Ed., A. Mishonov Technical Ed., NOAA Atlas NESDIS, 74, 39.